Acta Geochim (2018) 37(4):614–631
https://doi.org/10.1007/s11631-017-0257-0

ORIGINAL ARTICLE

Genesis of the Nanyangtian scheelite deposit in southeastern Yunnan Province, China: evidence from mineral chemistry, fluid inclusions, and C–O isotopes

Qianru Cai[1] · Yongfeng Yan[1] · Guangshu Yang[1] · Fuju Jia[1] · Chao Li[1]

Received: 19 April 2017 / Revised: 22 November 2017 / Accepted: 26 December 2017 / Published online: 16 January 2018

Abstract The Nanyangtian skarn-type scheelite deposit is an important part of the Laojunshan W–Sn polymetallic metallogenic region in southeastern Yunnan Province, China. The deposit comprises multiple scheelite ore bodies; multilayer skarn-type scheelite ore bodies are dominant, with a small amount of quartz vein-type ore bodies. Skarn minerals include diopside, hedenbergite, grossular, and epidote. Three mineralization stages exist: skarn, quartz–scheelite, and calcite. The homogenization temperatures of fluid inclusions in hydrothermal minerals that formed in different paragenetic phases were measured as follows: 221–423 °C (early skarn stage), 177–260 °C (quartz–scheelite stage), and 173–227 °C (late calcite stage). The measured salinity of fluid inclusions ranged from 0.18% to 16.34% NaCleqv (skarn stage), 0.35%–7.17% NaCleqv (quartz–scheelite stage), and 0.35%–2.24% NaCleqv (late calcite vein stage). Laser Raman spectroscopic studies on fluid inclusions in the three stages showed H_2O as the main component, with N_2 present in minor amounts. Minor amounts of CH_4 were found in the quartz–scheelite stage. It was observed that the homogenization temperature gradually reduced from the early to the late mineralization stages; moreover, $\delta^{13}C_{PDB}$ values for ore-bearing skarn in the mineralization period ranged from − 5.7‰ to − 6.9‰ and the corresponding $\delta^{18}O_{SMOW}$ values ranged from 5.8‰ to 9.1‰, implying that the ore-forming fluid was mainly sourced from magmatic water with a minor amount of meteoric water. Collectively, the evidence indicates that the formation of the Nanyangtian deposit is related to Laojunshan granitic magmatism.

Keywords Fluid inclusion · C–O isotopes · Skarn · Scheelite deposit · Nanyangtian

1 Introduction

The Laojunshan W–Sn metallogenic district is an important mineral resource base in Yunnan Province. Various W–Sn polymetallic deposits surround the Laojunshan granitic pluton: the Nanyangtian-Chayeshan W metallogenic belt in the east, the Dazhushan-Xinzhai Sn–W metallogenic belt in the north, and the Manjiazhai-Tongjie Zn–Sn–In metallogenic belt in the southwest. Ten years ago, a large Nanyangtian scheelite deposit containing high-grade ore with considerable prospecting potential was discovered; it has since been the subject of several studies. Previous research has focused on the geological setting, geochemistry, and fluid inclusions of minerals in this deposit and has produced a detailed chronology of events (Zeng et al. 1999; Shi et al. 2011; Wang et al. 2012; Feng et al. 2011a, b), thereby paving the way for further prospecting.

Previous work in the field of fluid inclusions includes: Feng et al. (2011a, b) work on quartz and garnet in the Nanyangtian scheelite deposit; Li (2013) research of fluid inclusions in quartz, garnet, and calcite in the Yanggouhe deposit; and Zhang et al.'s (2014) study of inclusions in skarn mineral and quartz in the Guanfang scheelite deposit using a thermometer and laser Raman spectrometer. Previous research on the source of ore-forming fluids and ore genesis by fluid inclusion analysis has not been comprehensive. As gangue minerals and ore minerals have

✉ Yongfeng Yan
yyf701018@vip.sina.com

[1] Kunming University of Science and Technology, Kunming 650093, China

different characteristics, the condition of ore minerals cannot be gleaned by analyzing gangue (Campbell and Robinson-Cock 1987; Campbell and Panter 1990; Giamello et al. 1992). All three publications mentioned above focused on the characteristics of fluid inclusions in gangue minerals rather than in ore; by analyzing fluid inclusions of ore minerals, the current work aims to provide more relevant information on the properties of metallogenic fluids.

Following a description of the geological setting and lithology of the Nanyangtian scheelite deposit, we discuss skarn mineralogical characteristics and the associated evolutionary process. Next, we report data from fluid inclusions in gangue and ore minerals, focusing particularly on the analysis of scheelite fluid inclusions. Finally, information about the ore-forming fluid and a logical explanation of the genesis of the Nanyangtian skarn scheelite deposit are provided.

1.1 Regional geology

Laojunshan is located at the intersection of the peri-Pacific and Tethyan Himalayan tectonic syntaxes and at the junction of the South China fold system, Ailaoshan fold system, North Vietnam Block, and Yangtze Plate (Fig. 1). The study area is in the southeastern Yunnan–western Guixi metallogenic belt, which lies to the west of the Nanling W–Sn polymetalloic metallogenic belt. Laojunshan therefore experiences frequent geologic activity, contains many active faults, and has excellent metallogenic conditions.

Because of a lack of upper Ordovician, Silurian, Jurassic, and Cretaceous strata, other strata are fully exposed in the area. According to lithology, the Laojunshan rock body can be divided into seven intrusive bodies: the Tuantian medium- to fine-grained granitic, Laochengpo fine-grained granitic, Huashitou two-mica adamellite, Malutang medium- to fine-grained two-mica adamellite, Taipingtou medium- to fine-grained two-mica adamellite, Qingjiao micrograin two-mica adamellite, and Kouha granite-porphyry intrusions. The Cambrian strata are exposed in the external contact zone of the Laojunshan rock body, which is mainly composed of schist, plagioclasite hornblende schist, amphibolite, and carbonate. Under magmatic hydrothermalism, carbonate altered to stratiform skarn, in which the scheelite ore body occurs.

The Cambrian strata comprise the Chongzhuang Formation in the Lower Cambrian series ($\epsilon_1$ch), and the Longha (ϵ_2l) and Tianpeng formations (ϵ_2t) in the Middle

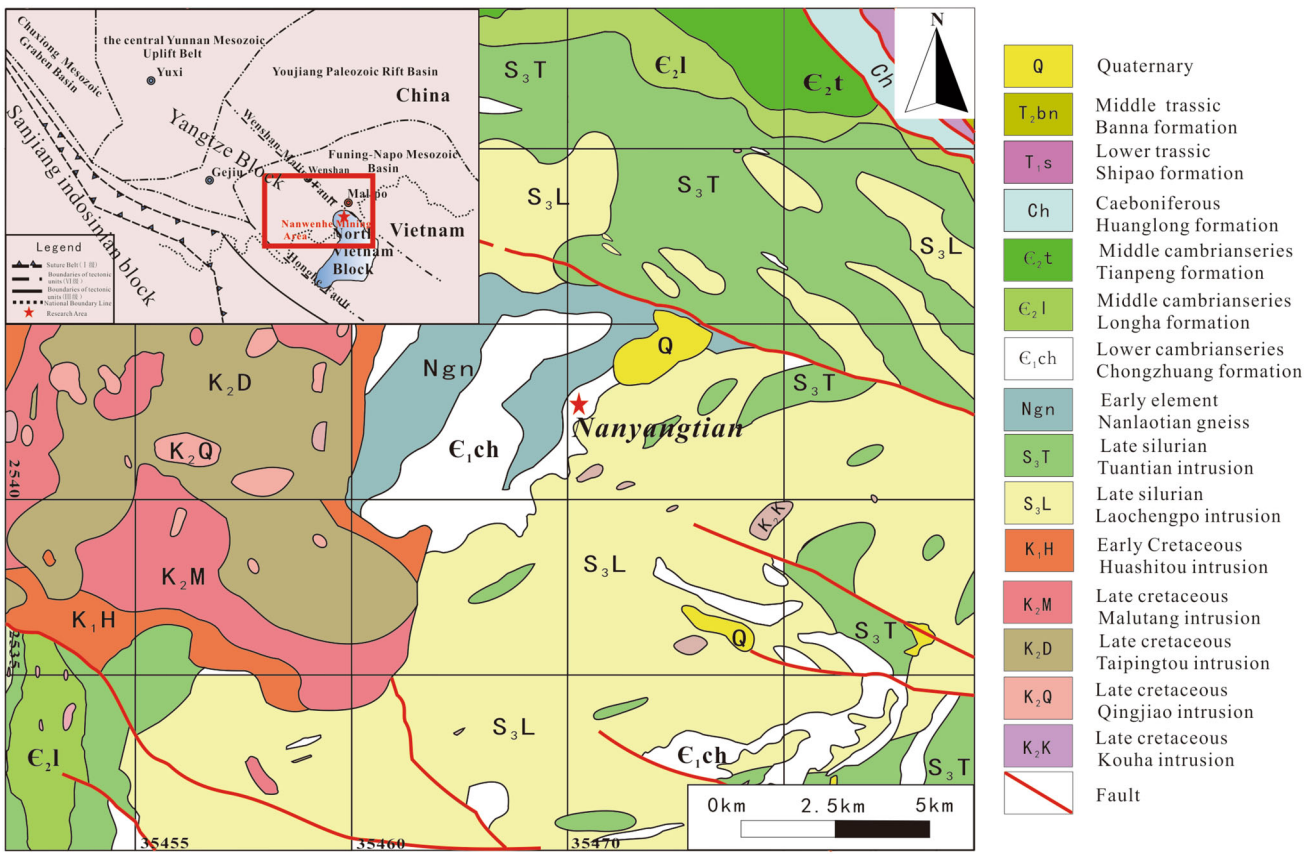

Fig. 1 Schematic tectonic map (**a**) and regional geological map (**b**) (after Zijin Tungsten Industry Group Co. LTD 2014)

Cambrian series. The Chongzhuang Formation exists mainly in the Nanyangtian mining area and can be classified into three lithologic members: the lower Geling section (ϵ_1ch^1), comprising granite gneiss and plagioclase gneiss; the middle Nanyangtian Section (ϵ_1ch^2), comprising verdelite biotite granulite, biotite plagioclase gneiss, two-mica schist, and tremolite-zoisite-diopside skarn; and the upper Taiyangping section (ϵ_1ch^3), comprising muscovite monzonitic gneiss. The Longha Formation is exposed mainly in Wenshan and Maguan as a hoary-white medium-embedded dolomite marble with a middle layer containing a small amount of phyllite and a bottom layer containing muscovite schist. The Tianpeng Formation occurs exclusively in the Dulong mining area. Its bottom layer is gneiss; its middle layer contains ore-bearing rocks mainly comprising actinolite, diopside, and chlorited skarn; and the rocks in its upper stratum are dolomitic phyllite, mica quartz schist, and interbedded marble (Jia 2010).

The Wenshan-Malipo Fault lies to the north of the Laojunshan granite body, the Maguan-Dulong Fault lies to the south, and the Nanwenhe Fault is an almost east–west direction. The secondary fault of Laojunshan provides conditions suitable for W–Sn ore formation. Regional metamorphism is strong, owing to multistage tectonism. A low-temperature regional dynamo metamorphism of granulite and schist occurred during the Caledonian-Indosinian. In addition, contact metamorphism occurred with the intrusion of Laojunshan granite during the Yanshanian, turning many early-deposited carbonate rocks into impure marble.

1.2 Geology of Nanyangtian scheelite deposit

In the mining area, the exposed strata are of the Lower Cambrian Chongzhuan Formation, outlined briefly above: ϵ_1ch^3 comprises muscovite-biotite plagioclase gneiss, muscovite-biotite schist, and tourmaline quartz schist with skarn lentils. Some parts of this section include mere granulite, and their thickness increases from the center margin. ϵ_1ch^2 consists mainly of ore-hosting strata. Its top is composed of thin biotite plagioclase gneiss and tourmaline feldspar quartzite; the middle of tourmaline biotite plagioclase gneiss, muscovite quartz schist, and phacoidal skarn; and the bottom of muscovite quartz schist, muscovite quartz schist with epidote tremolite skarn, and actinolite diopside skarn. ϵ_1ch^1 consists of granite gneiss and plagioclase gneiss with skarn lenticules, where skarn includes nonuniform and unstable dot and vein scheelite.

The main fault in the mining area is the Nanwenhe nappe structure, outcropping in the Nanyangtian District for approximately 10 km. The nappe structure is separated by the nappe fault in an imbricate arrangement consistent with direction of motion (from southeast to northwest). It is thought that the nappe fault may have been formed by the decoupling detachment of the Nanwenhe metamorphic core complex. The Nanyangtian sliding fracture is the highest sliding fracture within the nappe structure and is exposed to the east of the mining area near Nanyangtian. The southwest section of the fault is intruded by Dulong super-unit granite; the upper wall of the fault relates to the Laochengpo intrusion and contains Nanwenhe sequence gneissic fine-grained granite. The major fracture surface has strong mylonitization, and a quartz vein is sheared into a "Z" fold and a rootless fold by the fault. The hanging wall mainly consists of schist within the Chongzhuang Formation, and the cleavage tendency is southeast. The schist and gneiss have a small asymmetric fold plunging toward 200°–220° at an angle of 8°–15°.

The Yanshanian Laojunshan granitic pluton outcrops to the east of the mining area. Local igneous activity exhibits multiphase and multistage characteristics. Evolutionary periods (from ancient times to the current day) have resulted in three rock types: medium-coarse monzogranite, medium-fine monzogranite, and granite porphyry (the spread of which is reduced from the first rock body to the third, with the late-stage rock body intruding into the early rock body). The main part of the outcropped bedrock in the mining area is gneissic fine-grained granite porphyry with a mineral composition of 40% plagioclase, 40% quartz, and 10% biotite. The gneiss composition tends to be uniform and shows strong metasomatism. The rock has a metasomatic, relict, and perthitic texture. Although scheelite is not found in the granite, the W content is high.

All three stages of granites have relatively high Si (13.9%–70.4%), high A/NCK (1.11% to 1.26%), low Na_2O (< 4.0 wt%), and high K_2O (4.4 wt%–6.8 wt%). In ad'dition, they are enriched in P and depleted in Zr, Th, Y, and heavy rare earth elements, suggesting that Laojuanshan granites are S-type (Chappell 1999; Clemens 2003; Collins and Richards 2008; Xu 2015). The Nanyangtian phlogopite Ar–Ar average age is 118 Ma, consistent with the age of Laojunshan first-stage granites (Tan et al. 2011). From the above, tungsten mineralization and the first-stage Yanshanian granites are closely related (Liu et al. 2011).

The ore-bearing layer in the Nanyangtian mining area mainly occurs in the Nanyangtian section within the Lower Cambrian Chongzhuan Formation, where it lies within the upper, middle, and bottom strata. The ore body can be divided into skarn layers, a schist and gneiss layer, a quartz-tourmaline rock layer, and a schist and gneiss layer. Skarn-like rocks are embedded within granite gneiss from the top to the bottom of the strata. The ore body occurs in the bottom of the skarn-like layer and in the upper tourmaline-quartzite and gneiss layers (Figs. 2 and 3).

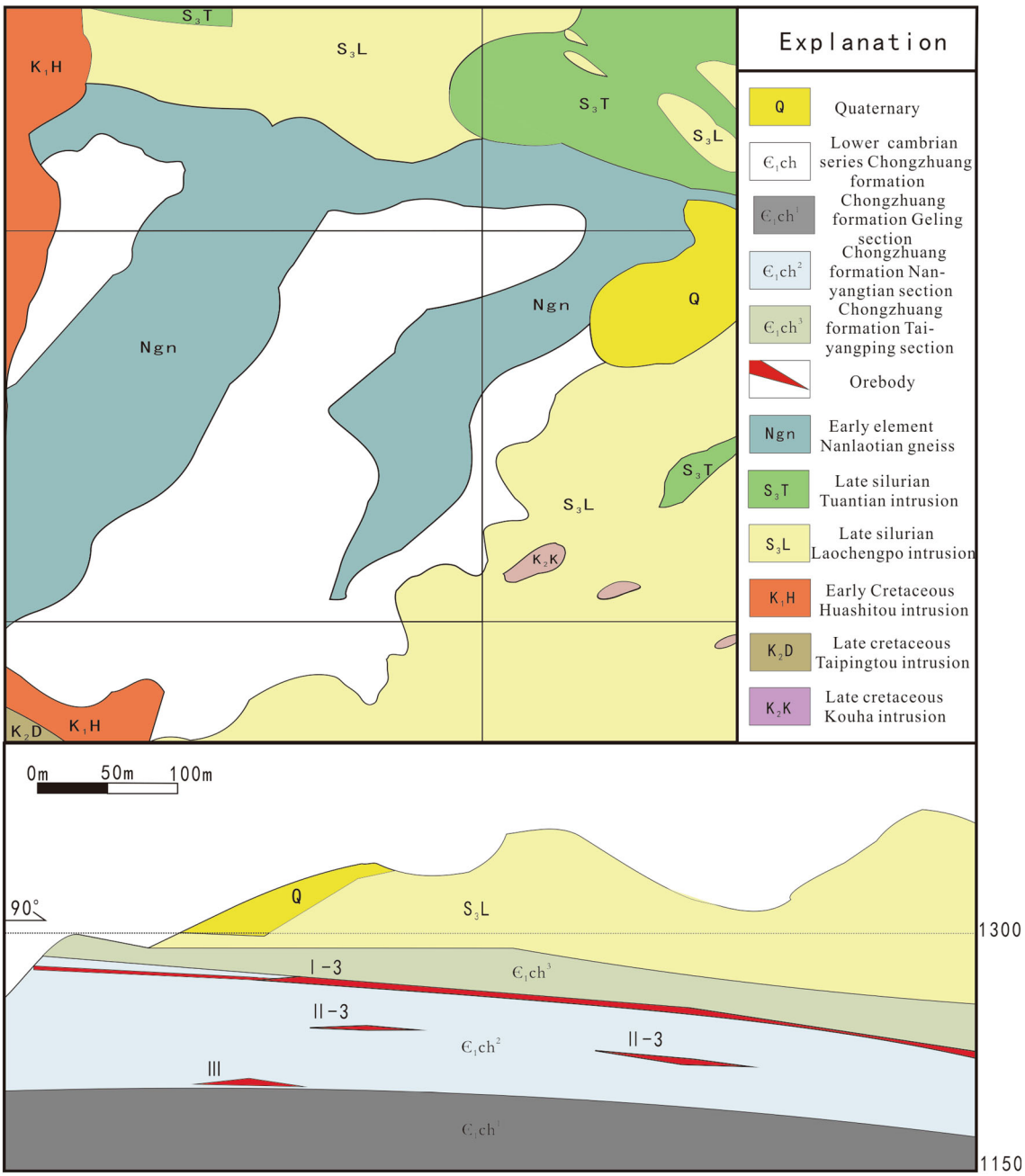

Fig. 2 mining area geological map (**a**) cross section A–B of Nanyangtian scheelite deposit (**b**) (after Zijin Tungsten Industry Group Co. Ltd, 2014)

According to the gallery sketch presented in Fig. 4, the following conclusions can be drawn. First, the shape of the ore body is generally stratiform or stratiform-like. The ore body is limited by the skarn, and the boundary is represented by spotted dissemination within the skarn. The quartz vein contains symbiotic vein-like scheelite and is very highly mineralized; W stems from the hydrothermal fluid. Second, in relation to the wall rock alteration characteristics, skarnization and siliconization are closely related to the mineralization of the surrounding rock, and the degree of mineralization is higher at locations where these processes have been more active. Third, according to the paragenetic association of minerals, the ore body layer is closely related to the genesis of skarn minerals and the vein ore body to the genesis of the quartz vein.

According to the interrelation of veins, ore texture and structure, and mineral assemblage, the mineralization stages can be divided into (1) the skarn stage, (2) the quartz–scheelite stage, and (3) the calcite stage. The skarn stage is characterized by garnet, diopside, tremolite, and

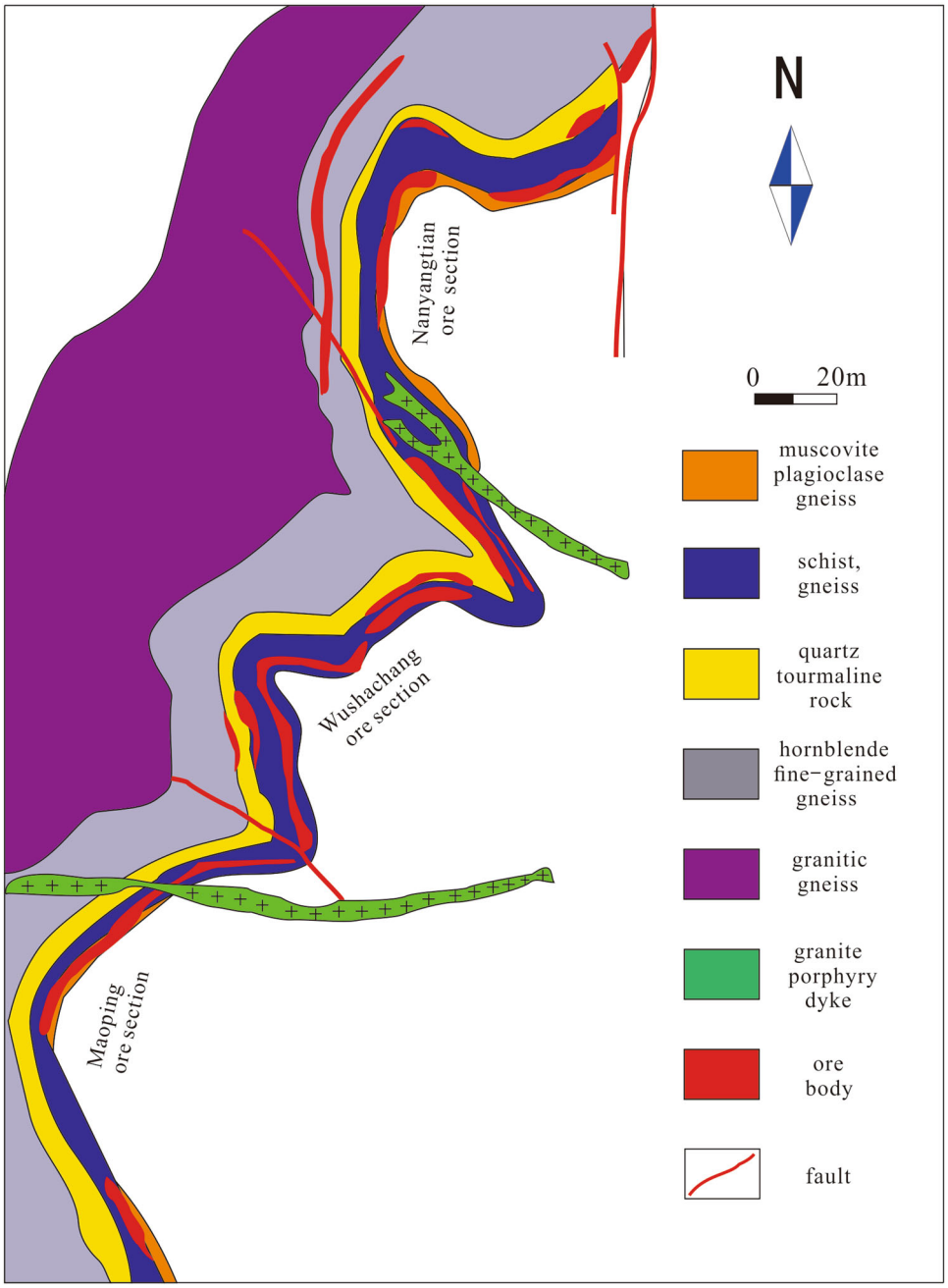

Fig. 3 The orebody distribution diagram of Nanyangtian scheelite deposit (after No 317 Geological Team of Yunnan, 1984)

epidote. The quartz–scheelite stage is characterized by quartz and scheelite. The calcite stage is characterized by calcite and sulfides, such as pyrite, chalcopyrite, and pyrrhotite (Fig. 5).

Skarn minerals observed in the Nanyangtian deposit include diopside, tremolite, zoisite, and garnet. Pyroxene was observed to be the main mineral in the Nanyangtian deposit skarn. Two types of pyroxene were observed in hand specimen: garnet at an early stage replaced by granular pyroxene, and pyroxene in a granular or stumpy form within skarn. Under a microscope, columnar and irregular pyroxene were observed in contact with garnet and hornblende (Fig. 6b, e). In addition, some pyroxene was noted to host fine-grained quartz and plagioclase, which impart a metasomatic relict texture. Rhombic dodecahedron or octahedron garnet crystals, rufous in color, were widespread. Garnet had experienced serious alteration, and scheelite was found between garnet crystals. Herein, zonation of garnet was observed using a microscope. Epidote is the most important hydrous skarn mineral observed in the deposit and formed by garnet alteration in the late skarn stage. Epidote was mainly seen as an idiomorphic-granular aggregate, colorful under the microscope, and occasionally replaced with pyroxene (Fig. 6c, f).

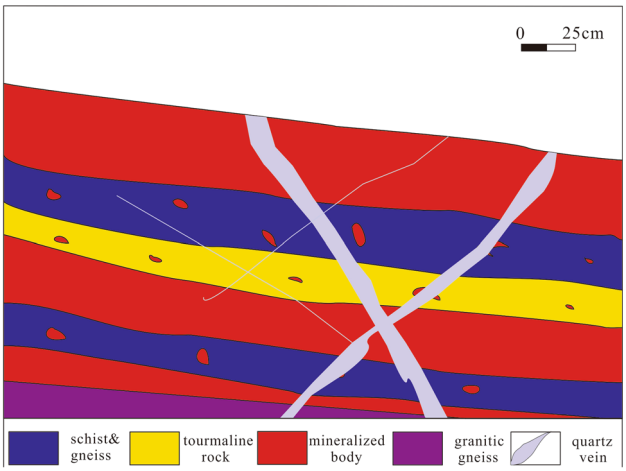

Fig. 4 Sketch ore body and wall rock contact relations in 1158 gallery 150 m

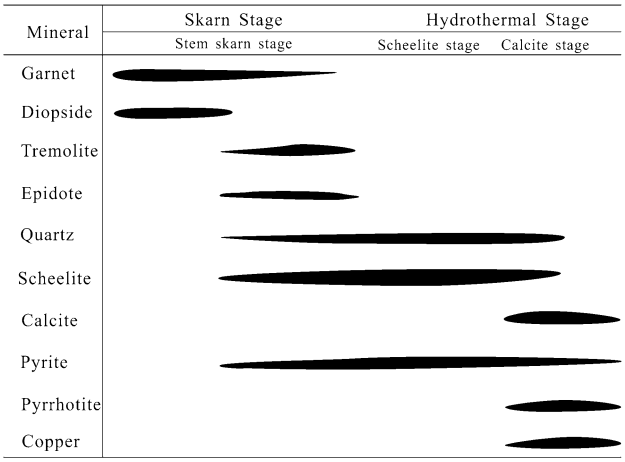

Fig. 5 Mineral-forming sequence in the NanYangtian deposit

Hornblende is another important hydrous skarn mineral found in the deposit (Fig. 6a, d) and was observed mainly as a radial or fibrous aggregate replacing pyroxene.

2 Sampling and analytical methods

Eight samples were collected from tunnels 25, 27, and 1158 in the Nanyangtian deposit. The samples collected contain diopside skarn, tremolite skarn, dioside-tremolite skarn, zoisite-diopside skarn, and garnet skarn. Electron microprobe analysis (EMPA) was performed for skarn minerals at Chang'an University using a JXA-8100 with an acceleration voltage of 15 kV and a beam current of 10 nA.

Samples were also collected from tunnels 27 and 1158 in the Nanyangtian ore district to analyze fluid inclusions. Fluid-inclusion analysis was conducted on samples containing garnet, epidote, quartz, and scheelite in the skarn stage; quartz and scheelite in the quartz–scheelite stage; and calcite in the calcite stage. The procedure involved polishing the samples into thin sections prior to observation with a microscope in order to determine differentiating forms, types, and distributions of fluid inclusions. Fluid-inclusion analysis was conducted using a Linkam THMSG-600 heating-freezing apparatus and a Renishaw inVia^{TM} laser Raman spectrometer installed on a Leica DM2500 M polarizing microscope at the Fluid Inclusion Laboratory of Kunming University of Science and Technology, Yunnan Province. A Spectra-Physics argon-ion laser was used to excite the laser Raman spectra with a 514.5-nm laser line at an incident power of 20 mW, spatial resolution of 1–2 μm, and an integral time of 60 s. The sample stage was connected to a thermal control unit to maintain the temperature in the range of 196–600 °C, and the measurements were considered accurate to ± 0.2 °C for ice-melting and CO_2 homogenization temperatures, ± 0.5 °C for clathrate melting temperatures, ± 1.5 °C for eutectic temperatures, and ± 5 °C for homogenization temperatures (Li et al. 2016a, b).

Five calcite samples were collected from the calcite vein of the Nanyangtian ore district for C–O isotope research. First, calcite samples were crushed and selected using a microscope. They were then powdered to a 200-mesh using an agate mill. C–O isotope analysis was then conducted using a Delta Plus XP continuous-flow isotope ratio mass spectrometer (CF-IRMS) at the Canada ALS mineral Laboratory (analytical precision was generally higher than 0.2‰).

3 Analysis results

3.1 Mineral chemistry analysis

3.1.1 Pyroxenes

Data on typical pyroxenes obtained from EMPA are shown in Table 1. The main components of pyroxene are diopside (55%–82%) and hedenbergite (18%–41%), with a small amount of johannsenite (0.3%–6%) (Fig. 7). As shown in Fig. 8, field-determined pyroxene components in the Nanyangtian deposit are typical of skarn deposits found throughout the world.

3.1.2 Garnet

The EMPA data obtained for typical garnet are shown in Table 2. In general, the end-member composition of garnet varies, providing important information about the formation environment (Ai and Jin 1981; Zhao et al. 1983;

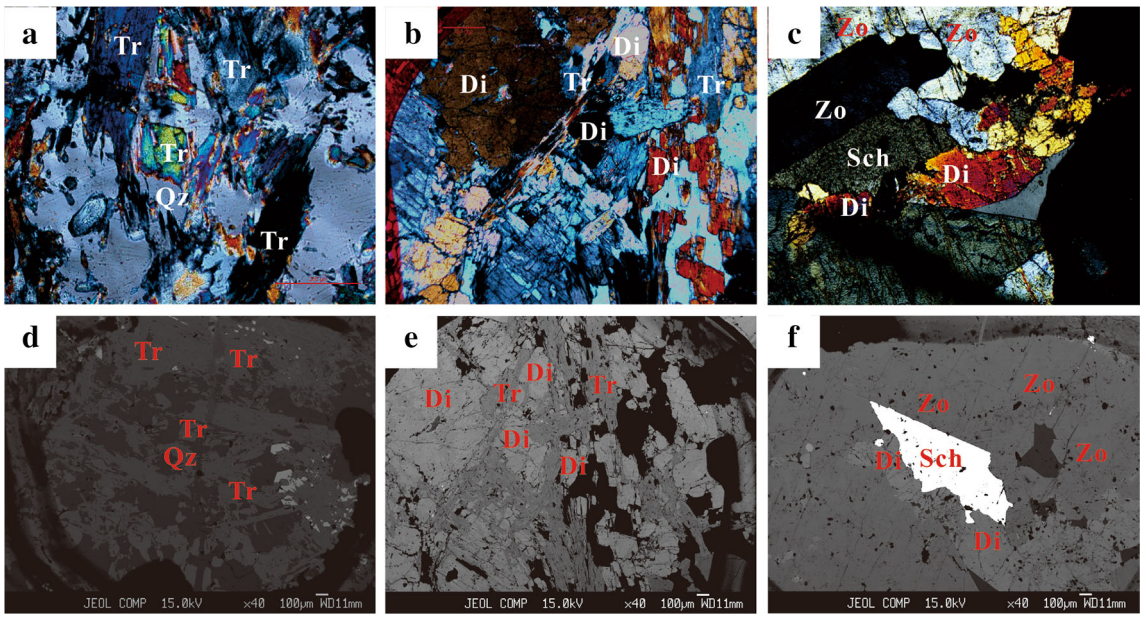

Fig. 6 Microphotograph of skarn minerals in the NanYangtian deposit; **a**, **d** tremolites of early stage replaced by quartz of late stage; **b**, **e** diopsides and tremolites dis-tributed in skarn; **c**, **f** scheelites is surrounded by diopsides and zoisites. *Qz* quartz, *Tr* tremolite, *Di* diopside, *Zo* zoisite, *Sch* scheelite

Meinert et al. 2005). As shown in Table 2, the endmember of Nanyangtian garnet samples was mainly grossular (Gro; 82.84%–88.51%) with some andradite (And; 3.61%–5.26%) and grossular (Alm + Spe + Pyr) (Fig. 8 and Fig. 9a), while the endmember of aluminum garnet samples was mainly almandine with small amounts of pyrope.

3.1.3 Epidote

The EMPA data obtained for typical epidote are shown in Table 3. The contents are as follows: SiO_2 ranges from 37.43% to 39.66% with an average of 38.78%, CaO from 22.71% to 23.15% with an average of 22.92%, Al_2O_3 from 25.53% to 29.84% with an average of 28.40%, and FeO_T from 4.31% to 8.64% with an average of 5.62%. Overall, epidote from the Nanyangtian deposit was Fe-poor with alumina-rich minerals. Figure 9b shows epidote mainly composed of clinozoisite with a small amount of piedmontite.

3.1.4 Hornblende

The EMPA data obtained for typical hornblende are shown in Table 4. The Al_2O_3 content ranges from 0.90% to 5.22%, CaO from 11.82% to 12.40%, FeO_T from 8.68% to 15.41%, MgO from 12.96% to 17.62%, and Na_2O from 0.11% to 0.78%. According to the standard classification (Leake et al. 1997), the hornblende within the Nanyangtian deposit plot determined in the field is of the tremolite-actinolite type (Fig. 10).

3.2 Fluid inclusion

3.2.1 Characteristics and microscopic temperature of fluid inclusions

Nanyangtian scheelite deposits can be mainly divided into three metallogenic stages: the skarn, quartz–scheelite, and calcite stages. Most Nangyangtian fluid inclusions are liquid-rich two-phase aqueous solutions (Lu et al. 2004). In this study, a homogenization temperature was observed when fluid inclusions were uniformly heated to a liquid phase, and a freezing-point temperature was observed when the temperature was lowered. Salinity was calculated using $W_{NaCl} = 0.00 + 1.78T_m - 0.0442T_m^2 + 0.000557T_m^3$ (Bodnar 1993), where W denotes the percentage composition of NaCl and T_m denotes the freezing-point temperature in Fahrenheit. Results are shown in Table 5.

3.2.1.1 Skarn stage Fluid inclusions of garnet, epidote, quartz, and scheelite in skarn were mainly two-phase aqueous inclusions; these were mainly observed and analyzed using temperature measurements (Fig. 11a–c). At room temperature (25 °C), the primary, secondary, and pseudo secondary inclusions were observed to be elliptical, long, or irregular. Secondary inclusions and pseudo secondary inclusions were mainly observed as negatives or

Table 1 EPMA composition of pyroxene from Nanyangtian scheelite deposit

Sample	1#	2#	3#	4#	5#	6#	7#	8#	9#	10#	11#	12#	13#	14#	15#
SiO_2	52.18	51.62	53.26	53.30	52.50	52.65	52.74	52.11	52.16	52.66	52.91	53.48	53.20	53.16	53.06
TiO_2	0.01	0.02	0.02	0.05	0.06	0.02		0.04	0.05	0.07	0.05	0.04	0.08	0.06	0.01
Al_2O_3	0.27	0.36	0.28	0.21	0.31	0.27	0.25	0.33	0.27	0.93	0.24	0.94	0.70	0.53	0.29
Cr_2O_3	0.05					0.09	0.11	0.06	0.03	0.08	0.02	0.03	0.48	0.01	0.10
FeO	12.28	11.64	10.13	9.81	11.61	10.80	11.58	12.60	12.19	8.68	9.90	5.62	6.50	7.31	9.04
MnO	1.76	1.19	1.06	1.39	1.18	1.14	1.52	1.21	1.58	0.31	0.25	0.08	0.09	0.11	0.82
MgO	10.08	10.32	11.28	11.12	10.35	10.81	10.13	9.52	9.86	12.02	11.43	14.27	13.11	13.68	11.21
CaO	23.09	22.66	22.97	23.16	22.99	23.24	22.93	22.85	22.98	23.23	23.51	23.82	23.57	23.78	23.43
Na_2O	0.13	0.06	0.13	0.12	0.04	0.08	0.06	0.12	0.11	0.19	0.10	0.12	0.18	0.19	0.03
K_2O		0.00	0.00				0.01	0.02		0.01	0.01	0.02	0.03	0.01	
Si	2.00	2.01	2.02	2.02	2.01	2.01	2.02	2.01	2.01	2.00	2.02	2.00	2.01	2.00	2.03
Al(vi)	0.01	0.02	0.01	0.01	0.01	0.01	0.01	0.02	0.01	0.04	0.01	0.04	0.03	0.02	0.01
Ti	0.00	0.00	0.00	0.00	0.00	0.00		0.00	0.00	0.00	0.00	0.00	0.00	0.00	0.00
Cr	0.00					0.00	0.00	0.00	0.00	0.00	0.00	0.00	0.01	0.00	0.00
Fe^{2+}	0.39	0.38	0.32	0.31	0.37	0.35	0.37	0.41	0.39	0.28	0.32	0.18	0.21	0.23	0.29
Mn	0.06	0.04	0.03	0.04	0.04	0.04	0.05	0.04	0.05	0.01	0.01	0.00	0.00	0.00	0.03
Mg	0.58	0.60	0.64	0.63	0.59	0.62	0.58	0.55	0.57	0.68	0.65	0.80	0.74	0.77	0.64
Ca	0.95	0.94	0.93	0.94	0.94	0.95	0.94	0.95	0.95	0.95	0.96	0.95	0.95	0.96	0.96
Na	0.01	0.00	0.01	0.01	0.00	0.01	0.00	0.01	0.01	0.01	0.01	0.01	0.01	0.01	0.00
K		0.00	0.00				0.00	0.00		0.00	0.00	0.00	0.00	0.00	
Wo	47.77	48.02	48.17	48.61	48.40	48.62	48.35	48.46	48.19	49.07	49.42	49.24	49.81	48.58	50.00
En	29.00	30.44	32.92	32.46	30.31	31.47	29.72	28.09	28.77	35.30	33.44	41.05	38.55	38.87	33.30
Fs	22.73	21.31	18.44	18.49	21.13	19.60	21.72	22.98	22.64	14.89	16.76	9.25	10.95	11.83	16.58
Ac	0.50	0.22	0.47	0.44	0.16	0.31	0.21	0.48	0.41	0.74	0.38	0.46	0.69	0.72	0.12
Di	0.56	0.59	0.64	0.64	0.59	0.62	0.58	0.55	0.56	0.70	0.67	0.82	0.78	0.77	0.67
Hd	0.38	0.37	0.32	0.32	0.37	0.35	0.37	0.41	0.39	0.29	0.33	0.18	0.22	0.23	0.30
Jo	0.06	0.04	0.03	0.05	0.04	0.04	0.05	0.04	0.05	0.01	0.01	0.00	0.00	0.00	0.03

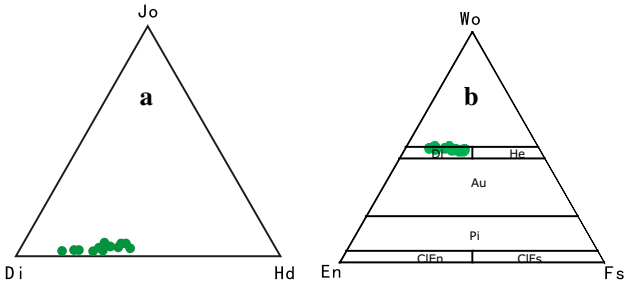

Fig. 7 Composition of pyroxene (**a**) and composition of pyroxene (**b**). *Jo* johannsenite, *Hd* hedenbergite, *Di* diopside, *Wo* wollaetonite, *En* magnesium enstenite, *Fs* iron enstenite, *Hd* hedenbergite, *Pi* pigeonite, *ClEn* Clinoenstatite, *ClFs* clinoferrosilite, *Au* augite

round crystals with a linear distribution. Two-phase aqueous inclusions were mainly colorless, with liquid/vapor ratios approximately 75% and lengths of 3–18 μm. The homogenization temperature of the inclusions in this stage ranged from 221 to 423 °C, with homogenization temperatures of garnet and epidote higher than those of quartz and scheelite. Salinity ranged from 0.18% to 16.34% (Fig. 12).

3.2.1.2 Quartz–scheelite stage The fluid inclusions observed in quartz included gas- and liquid-rich inclusions, with lengths of 5–30 μm and liquid/vapor ratios of approximately 75% (Fig. 11e). Most liquid-rich inclusions measured 10–18 μm, with very few up to 30 μm. Most two-phase inclusions were elliptical, long, or irregular. In addition, the fluid inclusions in scheelite were mainly two-phase, and mostly elliptical or irregular in shape, with length 3–14 μm (Fig. 12d) and liquid/vapor ratio greater than 85%. One-phase liquid inclusions were occasionally observed, usually in a clumped distribution and smaller than the two-phase inclusions. The homogenization temperatures of the inclusions in this stage ranged from 177 to 260 °C, with homogenization temperature of quartz higher than that of scheelite. Salinity ranged from 0.35% to 7.17% (Fig. 12).

Table 2 EPMA composition of garnet from Nanyangtian scheelite deposit

Sample	1#	2#	3#	4#	5#	6#	7#	8#	9#	10#	11#	12#
SiO_2	39.46	39.40	39.34	38.95	38.81	39.07	39.34	39.36	39.16	39.42	38.79	38.51
TiO_2	0.37	0.32	0.58	0.31	0.46	0.29	0.38	0.34	0.35	0.35	0.28	0.23
Al_2O_3	21.05	20.99	20.98	20.64	21.04	20.83	20.90	20.86	20.91	20.89	20.62	21.03
Cr_2O_3	0.00	0.00	0.00	0.00	0.03	0.00	0.00	0.12	0.00	0.08	0.00	0.02
FeO	5.23	5.23	4.25	5.37	4.39	5.14	5.36	5.55	4.89	5.90	5.46	5.21
MnO	1.09	1.24	0.34	0.82	0.34	1.04	1.49	1.47	0.90	1.37	1.33	1.85
MgO	0.11	0.11	0.08	0.08	0.15	0.10	0.10	0.13	0.07	0.11	0.09	0.10
CaO	32.25	32.06	33.09	31.88	32.83	32.00	32.18	31.89	32.07	31.70	31.03	31.88
Si	3.01	3.01	3.02	3.02	3.00	3.01	3.00	3.01	3.02	3.01	3.02	2.97
Ti	0.02	0.02	0.03	0.02	0.03	0.02	0.02	0.02	0.02	0.02	0.02	0.01
Al	1.89	1.89	1.90	1.88	1.92	1.89	1.88	1.88	1.90	1.88	1.89	1.91
Cr	0.00	0.00	0.00	0.00	0.00	0.00	0.00	0.01	0.00	0.00	0.00	0.00
Fe^{3+}	0.09	0.09	0.07	0.09	0.07	0.09	0.10	0.10	0.07	0.10	0.08	0.09
Fe^{2+}	0.25	0.25	0.20	0.26	0.22	0.25	0.24	0.26	0.24	0.28	0.27	0.24
Mn	0.07	0.08	0.02	0.05	0.02	0.07	0.10	0.10	0.06	0.09	0.09	0.12
Mg	0.01	0.01	0.01	0.01	0.02	0.01	0.01	0.01	0.01	0.01	0.01	0.01
Ca	2.64	2.63	2.72	2.65	2.72	2.64	2.63	2.61	2.65	2.59	2.59	2.64
Ura	0.00	0.00	0.00	0.00	0.10	0.00	0.00	0.36	0.00	0.23	0.00	0.07
And	4.33	4.36	3.61	4.68	3.29	4.35	5.26	4.98	3.69	4.94	4.14	4.63
Pyr	0.43	0.41	0.30	0.32	0.56	0.40	0.38	0.49	0.28	0.44	0.36	0.37
Spe	2.37	2.70	0.74	1.81	0.74	2.28	3.23	3.20	1.98	2.97	2.96	4.01
Gro	84.52	84.17	88.51	84.58	87.96	84.71	83.15	82.37	85.84	82.05	83.31	82.84
Alm	8.36	8.36	6.84	8.62	7.35	8.26	7.98	8.59	8.20	9.37	9.24	8.09

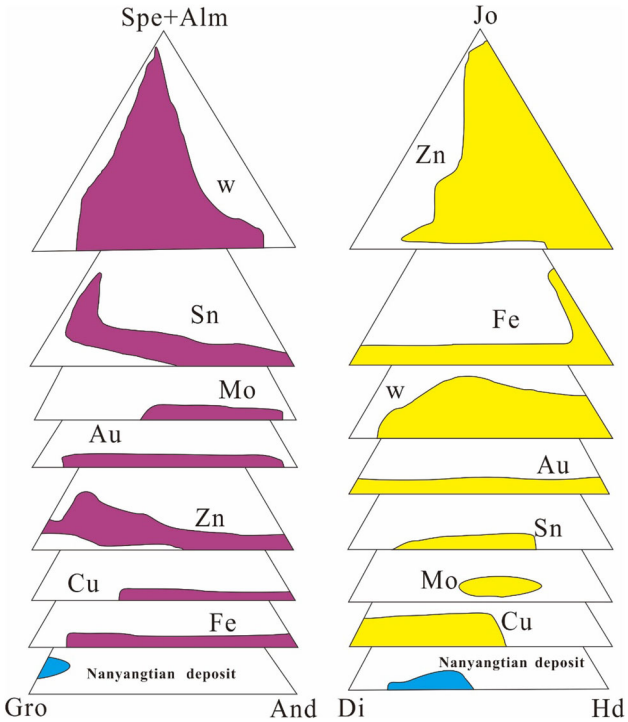

Fig. 8 Ternary plots of garnet and pyroxene compositions from major large skarn deposits (after Meinert 1992). *And* andradite, *Alm* almandine, *Spe* spessartite, *Gro* grossular, *Di* diopside, *Hd* hedenbergite, *Jo* johannsenite

3.2.1.3 Quartz–scheelite stage Fluid inclusions in calcite were mainly observed as two-phase, round, sporadically distributed aqueous inclusions, with liquid/vapor ratios greater than 90%, length 3–6 μm (Fig. 11f), homogenization temperatures of 173–227 °C, and salinity from 0.35% to 2.24% (Fig. 12).

Owing to the later metamorphism, the fluid inclusions of garnet in the early skarn stage are secondary inclusions; however, as they were destroyed, they could not contribute to the results of this study. In contrast, the fluid inclusions of epidote in the regressive alteration skarn stage were not destroyed and are composed of H_2O. In the quartz–scheelite stage, fluid inclusions generally displayed good integrity and a linear and clumped distribution. In general, the fluid inclusions in quartz were bigger than those in other stages. However, there was a lack of primary inclusions observed in scheelite. In addition, fluid inclusions in the calcite stage were less than 3 μm in length, making it difficult to obtain temperature readings.

3.2.2 Composition of fluid inclusions using laser Raman spectroscopy

In the skarn stage, the gas and liquid phases of the fluid inclusions in quartz and in epidote were composed of H_2O (Fig. 13g, h). In the quartz–scheelite stage; the composition of the gas and liquid phases of the representative fluid

Table 3 EPMA composition of epidote from Nanyangtian scheelite deposit

Sample	1#	2#	3#	4#	5#	6#	7#	8#	9#
SiO_2	37.65	38.79	39.04	38.70	38.85	38.44	39.59	37.86	38.72
TiO_2	0.07	0.14	0.10	0.16	0.12	0.14	0.33	0.07	0.07
Al_2O_3	28.31	28.07	28.95	28.23	28.46	27.42	29.30	28.13	28.95
Cr_2O_3	0.00	0.00	0.00	0.02	0.03	0.04	0.00	0.02	0.00
FeO	5.43	6.13	4.96	5.45	5.58	5.97	4.78	5.47	5.43
MnO	0.04	0.00	0.09	0.24	0.30	0.35	0.17	0.07	0.07
MgO	0.03	0.03	0.04	0.03	0.03	0.07	0.06	0.08	0.02
CaO	23.15	22.82	23.15	22.92	23.02	22.61	22.71	22.94	22.99
Na_2O	0.07	0.00	0.02	0.00	0.00	0.01	0.04	0.00	0.00
K_2O	0.00	0.00	0.02	0.00	0.00	0.00	0.00	0.00	0.00
Si	1.46	1.48	1.48	1.48	1.48	1.49	1.48	1.47	1.47
Al(iv)	0.54	0.52	0.52	0.52	0.52	0.51	0.52	0.53	0.53
Al(vi)	0.75	0.75	0.77	0.75	0.75	0.73	0.78	0.75	0.77
Ti	0.00	0.00	0.00	0.00	0.00	0.00	0.01	0.00	0.00
Cr	0.00	0.00	0.00	0.00	0.00	0.00	0.00	0.00	0.00
Fe2+	0.18	0.20	0.16	0.18	0.18	0.20	0.16	0.18	0.18
Mn	0.00	0.00	0.00	0.01	0.01	0.01	0.01	0.00	0.00
Mg	0.00	0.00	0.00	0.00	0.00	0.00	0.00	0.00	0.00
Ca	0.96	0.93	0.94	0.94	0.94	0.94	0.91	0.95	0.94
Na	0.01	0.00	0.00	0.00	0.00	0.00	0.00	0.00	0.00
K	0.00	0.00	0.00	0.00	0.00	0.00	0.00	0.00	0.00
Piedmontite	0.00	0.00	0.01	0.01	0.02	0.02	0.01	0.00	0.00
Epidote	0.00	0.00	0.00	0.00	0.00	0.00	0.00	0.00	0.00
Zoisite	1.00	1.00	0.99	0.99	0.98	0.98	0.99	1.00	1.00
Sample	10#	11#	12#	13#	14#	15#	16#	17#	18#
SiO_2	38.87	39.66	38.22	37.43	39.45	39.20	39.07	39.38	39.05
TiO_2	0.07	0.06	0.05	0.01	0.06	0.11	0.10	0.09	0.24
Al_2O_3	29.32	29.83	26.45	25.53	29.84	28.85	28.57	28.59	28.40
Cr_2O_3	0.00	0.00	0.02	0.00	0.09	0.00	0.00	0.00	0.00
FeO	4.31	4.71	8.15	8.64	4.84	5.66	5.39	5.16	5.05
MnO	0.00	0.15	0.11	0.00	0.01	0.23	0.00	0.09	0.16
MgO	0.02	0.01	0.02	0.05	0.06	0.05	0.04	0.07	0.06
CaO	23.16	22.77	22.92	22.72	22.99	23.01	22.78	23.09	22.81
Na_2O	0.08	0.01	0.00	0.00	0.00	0.00	0.01	0.01	0.03
K_2O	0.00	0.01	0.00	0.01	0.00	0.02	0.00	0.01	0.01
Si	1.47	1.48	1.48	1.48	1.47	1.48	1.49	1.49	1.49
Al(iv)	0.53	0.52	0.52	0.52	0.53	0.52	0.51	0.51	0.51
Al(vi)	0.78	0.79	0.69	0.67	0.79	0.76	0.77	0.76	0.76
Ti	0.00	0.00	0.00	0.00	0.00	0.00	0.00	0.00	0.01
Cr	0.00	0.00	0.00	0.00	0.00	0.00	0.00	0.00	0.00
Fe^{2+}	0.14	0.15	0.27	0.29	0.16	0.18	0.18	0.17	0.17
Mn	0.00	0.00	0.00	0.00	0.00	0.01	0.00	0.00	0.01
Mg	0.00	0.00	0.00	0.00	0.00	0.00	0.00	0.00	0.00
Ca	0.94	0.91	0.95	0.96	0.92	0.93	0.93	0.94	0.93
Na	0.01	0.00	0.00	0.00	0.00	0.00	0.00	0.00	0.00
K	0.00	0.00	0.00	0.00	0.00	0.00	0.00	0.00	0.00
Piedmontite	0.00	0.01	0.01	0.00	0.00	0.01	0.00	0.01	0.01
Epidote	0.00	0.00	0.00	0.00	0.00	0.00	0.00	0.00	0.00
Zoisite	1.00	0.99	0.99	1.00	1.00	0.99	1.00	0.99	0.99

Table 4 EPMA composition of hornblende from Nanyangtian scheelite deposit

Sample	1#	2#	3#	4#	5#	6#	7#	8#	9#	10#	11#	12#	13#	14#	15#
SiO_2	53.68	55.50	54.58	52.76	53.31	54.11	51.62	52.45	53.61	54.53	50.74	54.36	51.40	52.91	54.51
TiO_2	0.04	0.01	0.00	0.04	0.04	0.02	0.06	0.05	0.08	0.00	0.06	0.07	0.07	0.04	0.08
Al_2O_3	2.04	1.12	0.90	2.46	1.61	1.79	4.39	3.37	1.45	1.49	5.22	1.79	4.96	2.08	1.90
FeO	12.46	12.62	13.02	13.48	15.41	13.89	14.34	13.63	13.33	12.98	13.72	12.98	10.91	8.68	8.92
MnO	1.28	1.11	1.44	0.97	1.76	1.37	1.18	1.09	1.35	1.30	1.22	1.41	0.40	0.63	0.64
MgO	14.72	14.89	14.66	13.96	13.27	14.76	13.06	14.11	14.67	14.57	12.96	14.60	15.09	17.59	17.62
CaO	12.04	12.29	12.12	12.06	11.99	11.85	11.94	12.09	11.82	11.93	11.87	11.93	12.18	12.13	12.40
Na_2O	0.22	0.21	0.11	0.20	0.18	0.26	0.64	0.51	0.17	0.23	0.78	0.28	0.71	0.44	0.38
K_2O	0.09	0.05	0.07	0.20	0.08	0.15	0.23	0.25	0.10	0.13	0.30	0.14	0.35	0.07	0.06
Si	7.83	7.97	7.95	7.77	7.82	7.82	7.56	7.64	7.86	7.92	7.47	7.87	7.50	7.75	7.81
Al^{IV}	0.17	0.03	0.05	0.23	0.18	0.18	0.44	0.36	0.14	0.08	0.53	0.13	0.50	0.25	0.19
Al^{VI}	0.18	0.16	0.11	0.20	0.10	0.12	0.31	0.22	0.11	0.17	0.37	0.17	0.35	0.11	0.13
Ti	0.00	0.00	0.00	0.00	0.00	0.00	0.01	0.01	0.01	0.00	0.01	0.01	0.01	0.00	0.01
Fe^{3+}	0.97	1.04	1.01	0.94	0.93	0.92	0.83	0.84	0.96	1.00	0.79	0.97	0.80	0.86	0.92
Fe^{2+}	0.55	0.48	0.58	0.72	0.96	0.76	0.93	0.82	0.68	0.58	0.90	0.60	0.53	0.20	0.15
Mn	0.16	0.13	0.18	0.12	0.22	0.17	0.15	0.13	0.17	0.16	0.15	0.17	0.05	0.08	0.08
Mg	3.20	3.19	3.18	3.07	2.90	3.18	2.85	3.06	3.21	3.15	2.84	3.15	3.28	3.84	3.76
Ca	1.88	1.89	1.89	1.90	1.88	1.83	1.87	1.89	1.86	1.85	1.87	1.85	1.91	1.90	1.90
Na	0.06	0.06	0.03	0.06	0.05	0.07	0.18	0.14	0.05	0.07	0.22	0.08	0.20	0.12	0.11
K	0.02	0.01	0.01	0.04	0.02	0.03	0.04	0.05	0.02	0.02	0.06	0.03	0.06	0.01	0.01

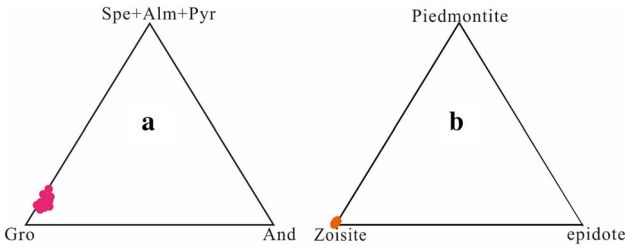

Fig. 9 **a** End members of garnets, **b** composition of epidote from the Nanyangtian scheelite deposit (*Gro* grossular, *And* andradite, *Spe* spessartite, *Alm* almandine, *pyr* pyrope)

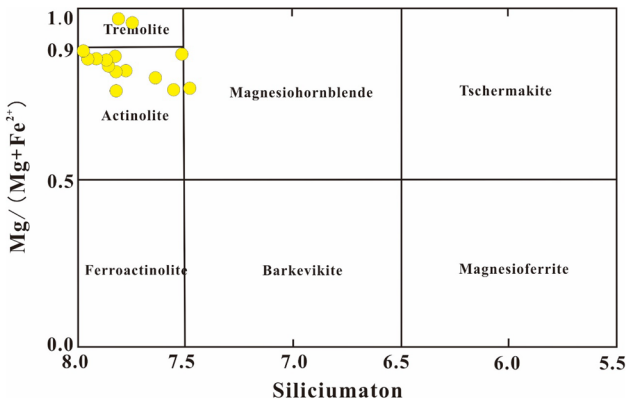

Fig. 10 Classification of amphiboles in the Nanyangtian deposit (base map after Leake et al. 1997)

inclusions of the first type of quartz was H_2O, N_2, and CO_2 (Fig. 13a, b); of the second type, H_2O and N_2 (Fig. 13c, d). The composition of the fluid inclusions in scheelite was H_2O, N_2, and CH_4 (Fig. 13e, f) and that of calcite, H_2O.

3.3 C and O isotopic composition

The C isotopic compositions of the calcite samples in the Nanyangtian deposits have a modest distribution ($\delta^{13}C_{PDB}$ was between − 5.7‰, and − 6.9‰, with an average value of − 6.3‰). However, the oxygen-isotope values of the calcite samples have a larger distribution ($\delta^{18}O_{SMOW}$ was between 5.8‰, and 9.1‰, with an average value of 7.45‰) (Table 6).

4 Discussion

4.1 Skarn type and formation environment

Skarn often forms within the metasomatic zone between intermediate intrusive rock and carbonate rock or between Ca/Mg enriched clastic rocks. It is generally believed that skarn is closely related to large amounts of metal accumulation (Zhao et al. 1990; Cheng and Zhao 1994); determining skarn type is significant because has implications for ore-bearing rock.

Table 5 Microthermometric data for fluid inclusions in the Nanyangtian tungsten deposit

Sample	Host diagenetic	Number	Size (μm)	Gas–liquid ratio (%)	Ice point ($T_m$ice) (°C)	Homogenization temperature (T_h) (°C)	Salinity (wt% NaCleqv)
Skarn	Garnet	12	3–9	5–15	− 6.3 to − 1.3	332–423	9.6–2.24
	Epidote	10	3–6	5–10	− 6.2 to − 3.9	287–367	9.47–6.30
	Quartz	26	4–18	5–25	− 12.4 to − 0.1	239–335	16.34–0.18
	Scheelite	6	3–8	5–25	− 2.2 to − 0.4	221–320	3.71–0.71
Quartz–scheelite	Quartz	36	5–31	5–30	− 4.5 to − 0.2	197–260	7.17–0.35
	Scheelite	12	3–14	5–15	− 2.5 to − 0.2	177–246	4.18–0.35
Calcite vein	Calcite	6	3–6	5–10	− 1.3 to − 0.2	173–227	2.24–0.35

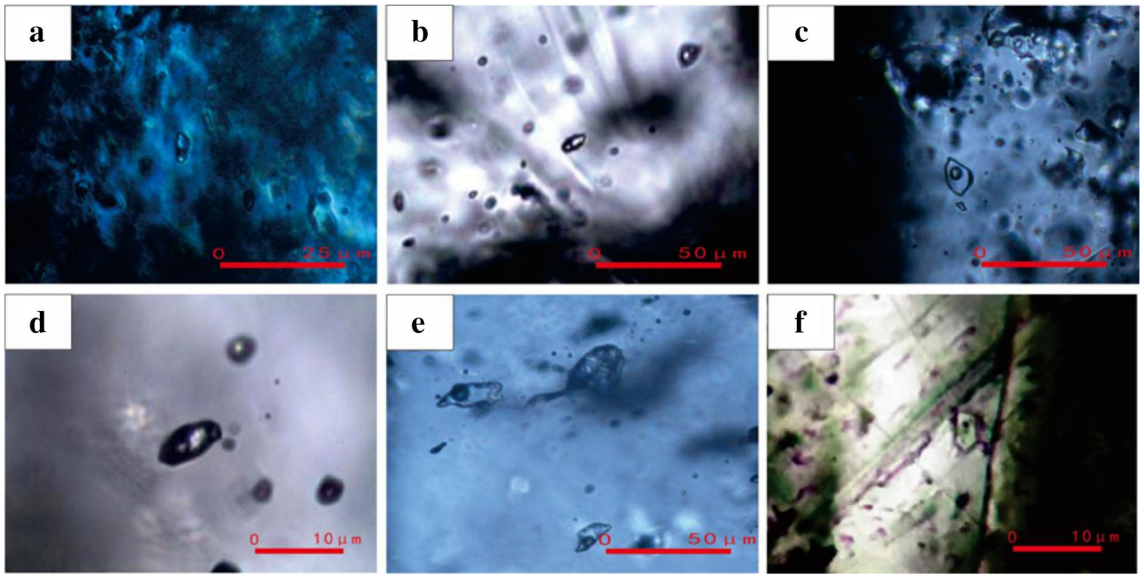

Fig. 11 Fluid inclusions in ore and gangue minerals of different altered stages of Nanyangtian scheelite deposit; **a** primary aqueous inclusion in the garnet from skarn; **b** primary aqueous inclusion in the epidosite from skarn; **c** primary aqueous inclusion in the quartz from quartz–scheelite vein; **d** primary aqueous inclusion in the scheelite from quartz–scheelite vein; **e** primary aqueous inclusion in the quartz from quartz–scheelite vein; **f** primary aqueous inclusion in the calcite from calcite vein

Based on mineral composition, skarn is categorized as either magnesium or calcium skarn (Einaudi et al. 1981). Magnesium skarn mainly consists of forsterite, diopside, spinel, phlogopite, and tremolite minerals, and the surrounding rock is dolomite. Calcium skarn mainly consists of andradite-grossularite, diopside-hedenbergite, wollastonite, scapolite, epidote, idocrase, and hornblende, and the surrounding rock is limestone. The mineral assemblage of the Nanyangtian deposit is mainly diopside + hedenbergite + grossularite + hornblende + epidote, indicating a primarily calcareous skarn.

During the process of skarn formation, the oxidation–deoxidation regime and the pH of the ore-forming fluid are very important for mineralization (Chen et al. 2012); moreover, the mineral composition of skarn provides important information about the ore-formation setting (Einaudi et al. 1981; Ahmed and Hariri 2006). Furthermore, the endmembers of garnet and pyroxene indicate the environment of skarn formation. Kwak (1994) and Lu et al. (2003) suggest that hessonite and hedenbergite usually form in a deoxidizing environment. The results of this study show that the end member of Nanyangtian garnet is mainly calcium–aluminum garnet and that the components of pyroxene are mainly diopside and hedenbergite. These results indicate that the early skarn stage occurred in a reducing environment.

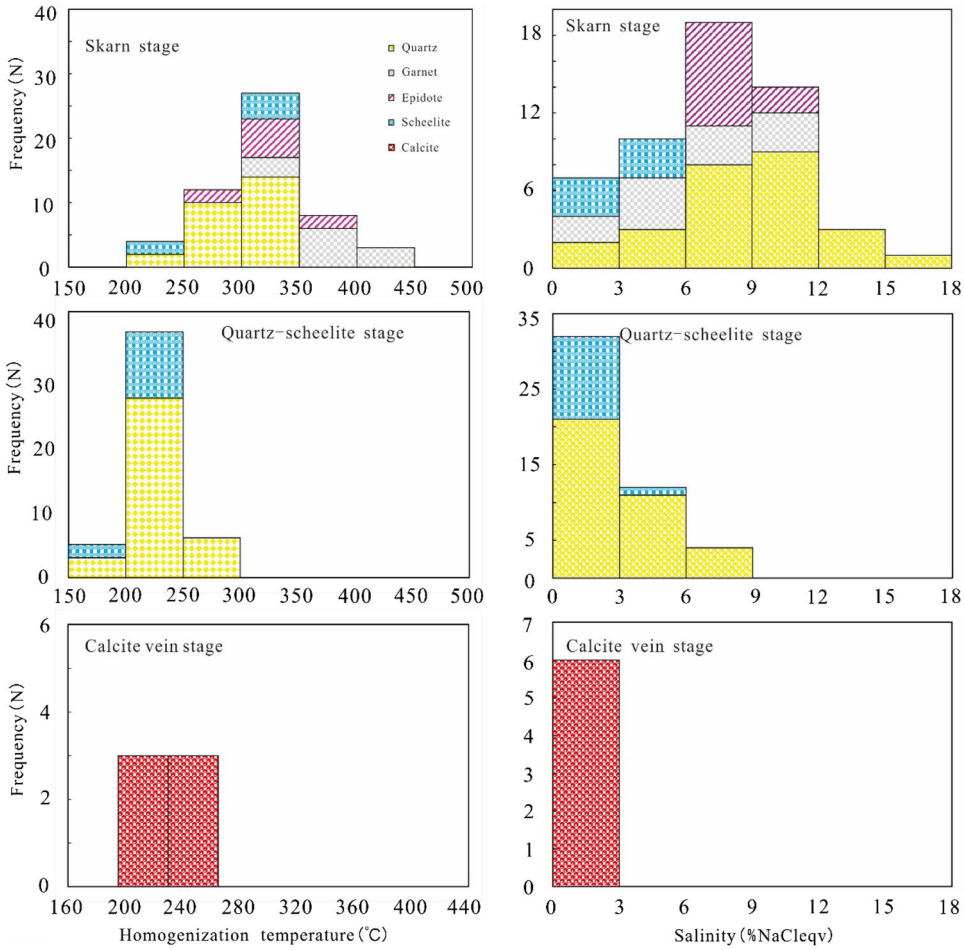

Fig. 12 Histogram of homogenization temperature and salinity in fluid inclusions from the Nanyangtian scheelite deposit

4.2 Nature and evolution of ore-forming fluids

Certain fluids can dissolve metallic elements; moreover, it is widely believed that they are effective carriers and transportation media for ore-forming elements (Li 2013). Scheelite in the Nanyangtian deposit spans skarn, quartz–scheelite, and calcite stages. In general, scheelite and Mo minerals are associated with each other, and the phenomena of rich W and deficient Mo mineralization in the Nanyangtian scheelite deposit suggest an ore-forming fluid with low oxygen fugacity (Candela and Bouton 1990). Under such conditions, a greater amount of W is transferred to the fluid phase during the magmatic crystallization process. Two distinct fluids were found in quartz inclusions of the Nanyangtian scheelite deposit: one containing CO_2, N_2, and H_2O (Fig. 13a, b) and the other only N_2 and H_2O (Fig. 13c, d)—an inhomogeneous fluid distribution. However, the low salinity of the fluid inclusions suggests a weak association between migration of scheelite in the Nanyangtian deposit and chlorine and fluorine content. The fluid inclusions within scheelite contained N_2, H_2O, and a certain amount of CH_4 (Fig. 13e, f). Although scheelite is a hypothermal ore-forming element, its actual ore-forming temperature is not high in some deposits, which is the main reason for tungstic acid migration in the ore-forming hydrothermal solution (Cattalani and Williams-Jones 1991; Wood and Samson 2000; Liu et al. 2008).

Thermometry data show that cooling occurred between the skarn and calcite stages, indicating a wide ore-forming temperature range for scheelite, similar to the thermal evolutionary history of other skarn scheelite deposits such as the CanTung and Kara scheelite ores (Singoyi and Zaw 2001). As shown in the homogenization temperature and salinity correlogram (Fig. 14), there is no obvious correlation between homogenization temperature and salinity. When a fluid experiences cooling, it may also experience mixing. The salinity of inclusions captured during different ore-forming periods within the Nanyangtian scheelite deposit ranged from 0% to 10% NaCleqv, consistent with the measurements of fluid inclusions in the Gannan scheelite ore (less than 10% Nacleqv) (Wang et al. 2012). The coexistence of vapor-rich and liquid inclusions indicates that fluid boiling was not a key factor in the ore-

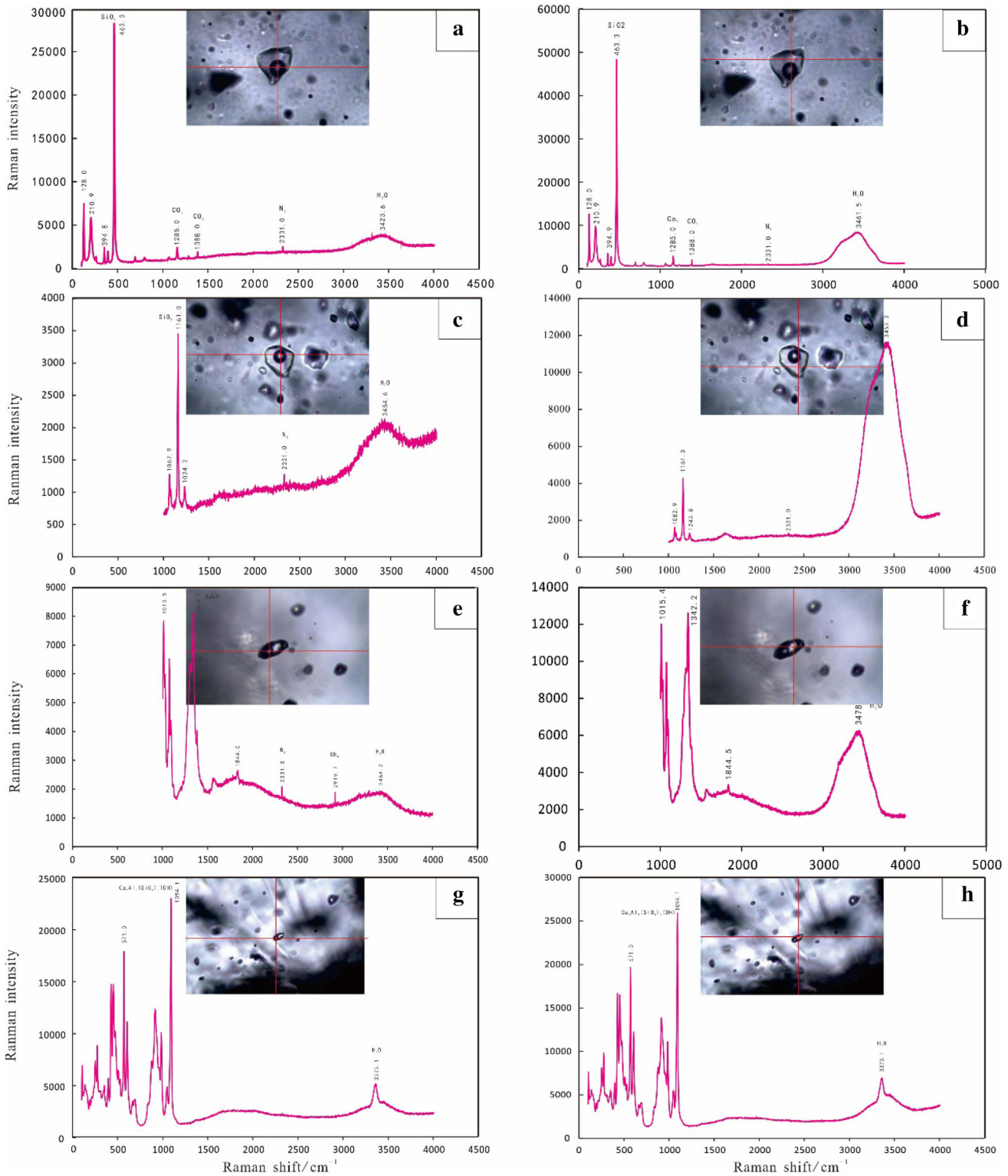

Fig. 13 Laser Raman spectra of fluid inclusions in the Nanyangtian scheelite deposit. **a**, **b**. Vapor and liquid phase composition of quartz inclusion. **c**, **d** Vapor and liquid phase composition of quartz inclusion. **e**, **f** Vapor and liquid phase composition of scheelite inclusion. **g**, **h** Vapor and liquid phase composition of epidosite inclusion

forming processes (Wu et al. 2014); therefore, researchers have concluded that scheelite ore formation partially depends on the wall rock type instead of on high Cl/H_2O content (Candela and Bouton 1990). However, the low salinity of the fluid inclusions in the ore and gangue minerals in the Nanyangtian scheelite deposit proves that the

Table 6 C–O isotopes of carbonates from Nanyangtian scheelite deposit

No.	Sample	Sample name	Mineral	$\delta^{13}C_{V\text{-}PDB}$ (‰)	$\delta^{18}O_{V\text{-}SMOW}$ (‰)
1	27-5-9	Calcite vein	Calcite	− 6.9	7.9
2	27-5-3	Calcite vein	Calcite	− 5.7	9.1
3	NYT-1	Calcite vein	Calcite	− 6.6	7.5
4	NYT-2	Calcite vein	Calcite	− 6.0	7.5
5	NYT-3	Calcite vein	Calcite	− 6.0	5.8

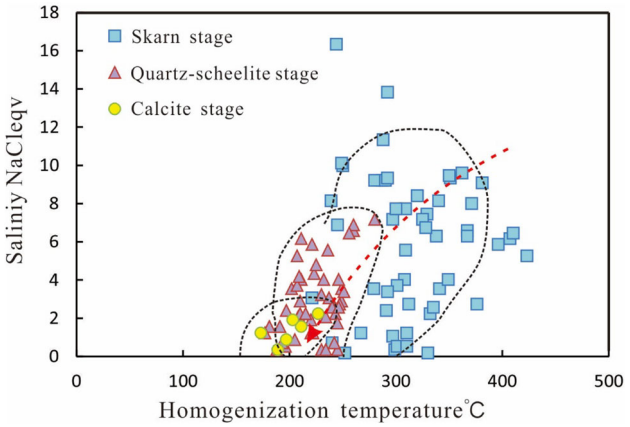

Fig. 14 Plot of homogenization temperatures versus salinities of fluid inclusion in Nanyagtian scheelite deposit

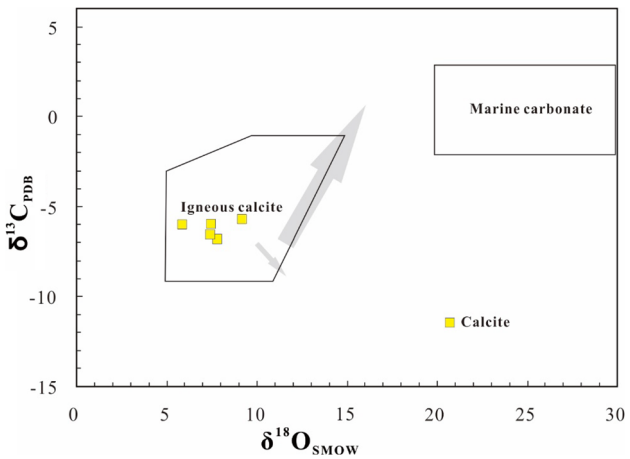

Fig. 15 $\delta^{18}O$–$\delta^{13}C$ diagram (after Ray et al. 2000)

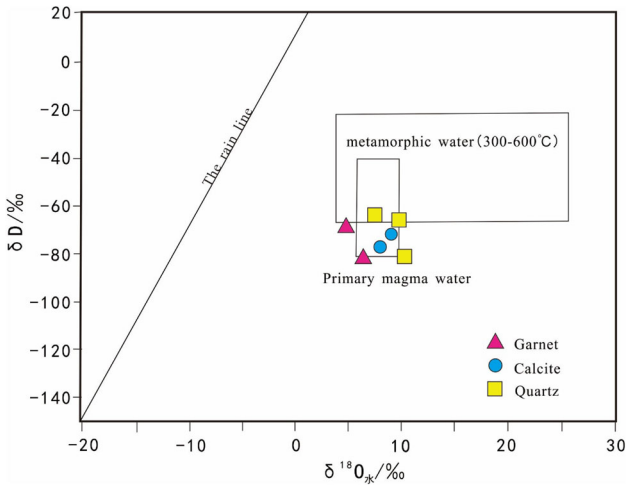

Fig. 16 δD versus $\delta^{18}O_{H2O}$ diagram of the Nanyangtian scheelite deposit (after Sheppard 1986)

metasomatic reaction between the scheelitic fluid and carbonatite was the mechanism for the formation of the scheelite deposit.

5 Source of ore-forming fluids

C–O isotopic systems have been widely used for tracing the source and evolution of ore-forming fluids (Zhou et al. 2013a, b). In general, carbon in hydrothermal fluids can be derived from the mantle, marine carbonate rocks, or sedimentary organic matter (Taylor et al. 1967; Veizer and Hoefs 1976; Demény and Harangi 1996; Liu and Liu 1997; Demény et al. 1998; Zhou et al. 2016). The mantle, marine carbonates, and organic matter have $\delta^{13}C_{PDB}$ values of − 4.0‰ to − 8.0‰ (Taylor et al. 1967), − 4.0 to + 4.0‰ (Veizer and Hoefs 1976), and − 30.0‰ to − 10.0‰ (Liu and Liu 1997), respectively and $\delta^{18}O_{SMOW}$ values of + 6.0‰ to + 10.0‰ (Taylor et al. 1967), + 20.0‰ to + 30.0‰ (Veizer and Hoefs 1976), and + 24.0‰ to + 30.0‰ (Liu and Liu 1997), respectively. The $\delta^{13}C_{PDB}$ values of calcite from Nanyangtian, compared with main natural carbon reservoirs, are consistent with those of mantle. In the $\delta^{13}C_{PDB}$ versus $^{18}O_{SMOW}$ diagram (Fig. 15), calcite samples from Nanyangtian fall into the area of igneous calcite. Meanwhile, the $\delta^{13}C_{PDB}$ values of calcite separates are also in accordance with those of magmatic source (from – 9‰ to 3‰, Li et al. 2016a, b), indicating an isotope exchange between granitic fluid and country-rock carbonate during the ore-forming processes.

As the main component of ore-forming fluid, water is one of the most researched topics in ore genesis (Wei et al. 2011). H and O isotopes have historically been used to trace the origin of ore-forming fluid of hydrothermal deposits (Deines 1980; Hoefs 1997; Pirajno 2009). Based on the measurement of H and O isotope values in garnet,

calcite, and quartz, Feng et al. (2011a, b) suggested that the water in ore formation is mainly magmatic, with a small amount of meteoric water, based on δD versus $\delta^{18}O_{H2O}$ diagrams (Fig. 16). In conclusion, C–O isotope features indicate that the calcite in ore-forming fluid is mainly derived from granitic magmatic water with a small amount of meteoric water, and H–O isotope features indicate that the water in ore formation mainly comes from magmatic water with a small amount of meteoric water.

5.1 Ore genesis and formation process

Previous studies have drawn different conclusions about the metallogenic mechanism. For example, Zeng et al. (1999) and Zhou et al. (1998) researched different types of scheelite rare earth elements and skarn and considered that the existence of scheelite in the Nanyangtian deposit to be related to metamorphic genesis. Feng et al. (2010, 2011) conducted comparative studies and determined that scheelite mineralization could be connected with magmatic movement during the Indo-Chinese epoch and that the formation of scheelite ore could be the result of a magmatic hydrothermal fluid reaction during the Indo-Chinese epoch. The Xianglushan scheelite deposit is representative of a magmatic hydrothermal-type skarn deposit. As the Nanyangtian scheelite deposit is of the same metallogenetic period and stage as the Xianglushan, this study compares their fluid geochemistry. The homogenization temperatures of the inclusions in the Xianglushan deposit at various stages are as follows. In the skarn stage: 209–383 °C, with a salinity of 0.35%–5.26% NaCleqv; in the quartz–scheelite stage: 163–278 °C, with a low salinity of 0.35%–5.86% NaCleqv; in the calcite stage: 143–235 °C, with a low salinity of 0.35%–2.07% NaCleqv (Wu et al. 2014). A comparison of the Xianglushan and Nanyangtian deposit inclusions shows similar homogenization temperatures and salinities; the Nanyangtian scheelite deposit has characteristics similar to those of a magmatic hydrothermal-type skarn deposit. The results of the field work and experiments conducted in this study show that scheelite mineralization occurred in the Laojunshan granite body and that it underwent multiphase ore formation. Previous studies have discussed the genesis of the Laojunshan granite body and concluded that it was formed by partial fusion of the lower crust rock, where hot mantle material upwelling was triggered during the Late Yanshanian (Liu et al. 2014). This conclusion is in accordance with the evidence provided by the present study on C and O isotopes and ore-forming fluids. The skarn W–Sn deposit is generally considered to be closely related to granites. Granitic magma is mainly related to a molten continental crust, which occurs during an intraplate rift (Richards 2011) when the continental crust is thicker owing to an earlier collision. It then experiences an extensional setting, during which the underplating of mantle-derived magma and direct heating of the asthenosphere crust cause the overlying lower crust materials to partially melt and form Nanyangtian primary magma (Hildreth 1981). In general, continental crust provides all or most of the metal, and the W–Sn deposit is related to S-type granite (Hedenquist and Lowenstern 1994; Mao et al. 2011). As shown in Fig. 8, garnet components in the Nanyangtian deposit are not in the range of typical skarn deposits found throughout the world. This indicates that garnet having high aluminum and low iron contents formed through a metasomatic reaction between minerals and S-type granitic magmatic hydrothermal fluids.

The nappe structure not only causes spatial super-positioning of the granite and the granulite but also causes shear sliding of the rock strata, which forms an interlayer fracture zone. The fracture zone is not only a migration pathway for ore-forming fluids but also provides an important host space. Through this migration channel, the acidic fluid migrates to the carbonate formations that formed during the early stage when metasomatism was completed (Bi et al. 2015).

The conclusions that follow are based on analyses of the material composition during the mineralization stage and the fluid properties. Mantle magma upwelled at an early stage and was stored at the bottom of the crust. The mantle heat source led to large-scale metamorphism and anatexis in the lower crust, which then formed a mass of granitic magma that crystallized and cooled as a result of the exsolution of Fe–Al-rich fluid. Garnet skarn and diopside skarn were formed by the metasomatism of a fluid with a temperature higher than that of the surrounding rock, consequently releasing a tungstate fluid. The temperature of this fluid was subsequently lowered during a reaction with the country rock, which caused scheelite to subside and mineralize. As the rock mass cooled, the released fluid partially transformed into Si–W–H_2O and continued to overflow. Vein-like faults formed between the skarn and the wall rock in relation to pressure; moreover, a vein ore body formed, which is why the vein-like quartz–scheelite ore overlies the skarn. Late stage Ca-rich fluid migrated along large faults and in-filled to form calcite veins.

6 Conclusion

Based on previous research, we analyzed fluid inclusions and measured C–O isotopes to determine the genesis of metal ores, the source of ore-forming fluids, and the metallogenic mechanism involved in the formation of skarn minerals within the Nanyangtian scheelite deposit. The following conclusions are drawn:

(1) Early-stage skarn was formed in a reducing environment.
(2) Early- to late-stage mineralization occurred over a wide temperature range.
(3) The metasomatic reaction between the scheelitic fluid and carbonatite was the effective mechanism underlying the formation of the scheelite deposit.
(4) Based on fluid inclusion analysis and the results of stable isotope tracing, ore-forming fluids of the Nanyangtian scheelite deposit are mainly related to a magmatic source and contain both stratigraphic water and atmospheric precipitation.
(5) The Nanyangtian deposit evolved through the Caledonian and Indo-Chinese but was formed by Laojunshan granite through magmatic contact and metasomatic action during the Yanshanian period.

Acknowledgements This study was supported by the Natural Science Foundation of China (No. 41373050). The authors are extremely grateful for the support and help provided by staff of the Nanyangtian ore deposit.

References

Ahmed Z, Hariri MM (2006) Formation and mineral chemistry of a calcic skarn form Al-madhiq, SW Saudi Arabia. Chenie der Erde Geochemistry 66:187–201

Ai YF, Jin LN (1981) The study of the relationship between the mineralization and the garnet in the skarn ore deposits. Acta Scientirum Naturalum Universitis Pekinesis 1:83–90

Bi MF, Zhang D, Wu GG, Di YJ, Que CY, Pan JB, Xue W (2015) Mesozoic tectonic deformation and ore-controlling of tungsten polymetallic deposits in Malipo area, southeastern Yunnan. Earth Sci Front 22(4):223–238

Bodnar RJ (1993) Revised and equation and table for determining the freezing point depression of H2O-NaCl solutions. Geochim Cosmochim Acta 57(3):683–684

Campbell AR, Panter KS (1990) Comparison of fluid inclusions in coexisting (cogenetic) wolframite, cassiterite and quartz from St. Michael's Mount and Cligga Head, Cornwall, England. Geochim Cosmochim Acta 54(3):673–681

Campbell AR, Robinson-Cook S (1987) Infrared fluid inclusion microthermometry on coexisting wolframite and quartz. Econ Geol 82(6):1640–1645

Candela PA, Bouton SL (1990) The influence of oxygen fugacity on scheelite and molybdenum partitioning between silicate melts and ilmenite. Econ Geol 85(3):633–640

Cattalani S, Williams-Jones AE (1991) C–O–H–N fluid evolution at Saint-Robert, Quebec: implications for W–Bi–Ag mineral deposition. Can Mineral 29(3):435–452

Chappell BW (1999) Aluminium saturation in i- and s-type granites and the characterization of fractionated haplogranites. Lithos 46(3):535–551

Chen L, Qin KZ, Li GM, Li JX, Xiao B, Jiang HH, Zhao JX, Fan X, Jiang SY (2012) Geological and skarn mineral characteristics of Nuri Cu–W–Mo deposit in southeast Gangdese. Tibet 31(3):417–437

Cheng YQ, Zhao YM (1994) China iron deposit. Geology Publishing House, Beijing, pp 386–479

Clemens JD (2003) S-type granitic magmas—petrogenetic issues, models and evidence. Earth Sci Rev 61(1–2):1–18

Collins WJ, Richards SW (2008) Geodynamic significance of s-type granites in circum-Pacific orogens. Geology 36(7):559–562

Dai J, Zhang LK, Pan XD, Shi HZ, Chen MH, Wang P, Zhang BH, Zhang Q, Jin B, Ren J (2011) Mineralogical characteristics and genesis discussion of skarn in Nanyangtian scheelite deposit of southeastern Yunnan. Rock Miner Anal 30(3):269–275

Deines P (1980) Stable isotope geochemistry. Stable isotope geochemistry. Springer, Berlin

Demény A, Harangi SZ (1996) Stable isotope studies on carbonate formations in alkaline basalt and lamprophyre series: evolution of magmatic fluids and magma–sediment interactions. Lithos 37:335–349

Demény A, Ahijado A, Casillas R, Vennemann TW (1998). Crustal contamination and fluid/rock interaction in the carbonatites of Fuerteventura (Canary Islands, Spain): C, O, H isotope study. Lithos 44:101–115

Einaudi MT, Meinert LD, Newberry RJ (1981) Skarn deposits. Econ Geol 75:317–391

Feng JR, Mao JW, Pei RF, Zhou ZH, Yang ZX (2010) U-Pb chronology in zircon form Laojunshan granitic pluton in Wazha Yunnan. Acta Petrol Sin 26(3):845–857

Feng JR, Mao JW, Pei RF, Li C (2011a) A tentative discussion on Indosinian ore-froming events in Laojunshan area of Southeastern: a case study of Xinzhai tin deposit and Nanyangtian scheelite deposit. Mineral Depos 30(1):57–73

Feng JR, Mao JW, Pei RF, Li C (2011b) Ore-forming fluids and metallogenesis of Nanyangtian scheelite deposit in Laojunshan, southeastern Yunnan Province. Miner Depos 30(3):403–419

Geological unit in Yunnan province (1984) Nanyangtian scheelite deposit deep evaluation report in the Malipo. Yunnan 16–77

Giamello M, Protano G, Riccobono F, Sabatini G (1992) The W–Mo deposit of Perda Majori (SE Sardinia, Italy): a fluid inclusion study of ore and gangue minerals. Eur J Mineral 4:1079–1084

Hedenquist JW, Lowenstern JB (1994) The role of magmas in the formation of hydrothermal ore deposits. Nature 370(6490):519–527

Hildreth W (1981) Gradients in silicic magma chambers: implications for lithospheric magmatism. J Geophys Res Solid Earth 86(B11):10153–10192

Hoefs J (1997) Stable isotope geochemistry. Springer, New York

Jia FJ (2010) Researches on metallogenic series and metallogenic regularities in Laojunshan metallogenic belt, Yunnan province pp 2–127

Kwak TA (1994) Hydrothermal alteration in carbonate replacement deposits. Geol Assoc Canada Short Course Notes 11:381–402

Leake BE, Woolley AR, Arps CE (1997) Nomenclature of amphiboles: report of the subcommittee on amphiboles of the international mineralogical association, commission on new mineral and mineral names. Am Miner 82:1019–1037

Li Y (2013) Research on fluid mineralization of skarn scheelite deposit of Yunnan province Malipo County Gouyanghe Mining area. China University of Geosciences (Beijing) pp 1–51

Li XF, Huang C, Wang C, Wang L (2016a) Genesis of the Huangshaping W–Mo–Cu–Pb–Zn polymetallic deposit in southeastern Hunan Province, China: constraints from fluid inclusions, trace elements, and isotopes. Ore Geol Rev 79:1–25

Li W, Xie GQ, Zhang ZY, Zhang XK (2016b) Constraint on the genesis of Gutaishan gold deposit in central Hunan Province: evidence from fluid inclusion and C-H-O isotopes. Acta Petrol Sin 32(11):3489–3506

Liu JM, Liu JJ (1997) Basin fluid genetic model of sediment-hosted micro-disseminated gold deposits in the gold-triangle area between Guizhou, Guangxi and Yunnan. Acta Mineral Sin 17:448–456 (in Chinese with English abstract)

Liu JJ, Liu GZ, Liao YF, Zheng WJ, Yue LX, Hua SG, Mao GJ, Wu SH (2008) Discovery and significance of scheelite orebodies in the Zhaishang gold deposit, southern Gansu. Geol China 35(6):1113–1120

Liu YP, Li ZX, Ye L, Tan HQ, Li CY (2011) Ar-Ar chronology of the Laojunshan Ore Concentrated Area in Southeast Yunnan Province. Acta Mineral Sin (s1):617–618

Liu YB, Mo XX, Zhang D, Que CY, Di YJ, Pu XM, Cheng GS, Ma HH (2014) Petrogenesis of the Late Cretaceous granite discovered in the Laojunshan region, southeastern Yunnan Province. Acta Petrol Sin 30(11):3271–3286

Lu HZ, Liu YM, Wang CL (2003) Mineralization and fluid inclusion study of the Shizuyuan W–Sn–Bi–Mo–F Skarn deposit, Hunan, Province, China. Econ Geol 98:955–974

Lu HZ, Fan HW, Ni P, Ou GX, Shen K, Zhang WH (2004) Fluid inclusions. Science Press, Beijing, pp 1–485

Mao JW, Chen MH, Yuan SD, Guo CL (2011) Geological characteristics of the Qinhang (or Shihang) metallogenic belt in South China and spatial-temporal distribution regularity of mineral deposits. Acta Geol Sin 85(5):636–658

Meinert LD (1992) Skarns and skarn deposits. Geosci Can 19:145–162

Meinert LD, Dipple GM, Nicolescu S (2005) World skarn deposits. Econ Geol 100th anniversary volume pp 299–336

Ohmoto H (1986) Stable isotopes geochemistry of ore deposits. Rev Miner Geochem 16:491–559

Pirajno F (2009) Hydrothermal processes and mineral systems. Springer, Amsterdam

Ray JS, Ramesh R, Pande K, Trivedi JR, Shukla PN, Patel PP (2000) Isotope and rare earth element chemistry of carbonatite-alkaline complexes of deccan volcanic province: implications to magmatic and alteration processes. J Asian Earth Sci 18(2):177–194

Richards JP (2011) Magmatic to hydrothermal metal fluxes in convergent and collided margins. Ore Geol Rev 40:1–25

Sheppard SMF (1986) Characterization and isotopic variations in natural waters. Rev Miner 16:165–183

Shi HZ, Zhang LK, Ren GM, Liu SS, Zhang B, Dai J, Chen MH (2011) The genesis of skarnoid form the Nanyangtian strata-bound scheelite deposit in Malipo, Yunnan Province. Geol China 38(3):673–680

Singoyi B, Zaw K (2001) A petrological and fluid inclusion study of magnetite-scheelite skarn mineralization at Kara, Northwestern Tasmania: implication for ore genesis. Chem Geol 173(1–5):239–253

Tan HQ, Liu YP, Ye L, Li CY (2011) Ar–Ar chronology of the Nanyangtian W-Sn Deposit in Southeast Yunnan Province, and Its Geological Significance. Acta Mineral Sin (s1):639–640

Taylor JHP, Frechen J, Degens ET (1967) Oxygen and carbon isotope studies of carbonatites from the Laacher See District, West Germany and the Alno District Sweden. Geochim Cosmochim Acta 31:407–430

Veizer J, Hoefs J (1976) The nature of $^{18}O/^{16}O$ and $^{13}C/^{12}C$ secular trends in sedimentary carbonate rocks. Geochim Cosmochim Acta 40:1387–1395

Wang G (2011) Characteristic and tracer action of rare earth elements Nanyangtian scheelite mining, Malipo, Yunnan pp 1–46

Wang XD, Ni P, Yuan SD, Wu SH (2012) Fluid inclusion studies of the Huangsha quartz-vein type scheelite deposit, Jiangxi Province. Acta Petrol Sin 28(1):122–132

Wei WF, Hu RZ, Peng JT, Bi XW, Song SQ, Shi SH (2011) Fluid mixing in Xihuashan tungsten deposit, Southern Jixangxi Province: hydrogen and oxygen isotope simulation analysis. Geochimica 40(1):45–55

Wood SA, Samson IM (2000) The hydrothermal geochemistry of scheelite in granitoid environments: i. Relative solubilities of ferberite and scheelite as a function of T, P, pH, and M NaCl. Econ Geol 95(1):143–182

Wu SH, Wang XD, Xiong BK (2014) Fluid inclusion studies of the xianglushan skarn tungsten deposit, Jiangxi province, china. Acta Petrol Sin 30(1):178–188

Xu B (2015) Multi-stage magmatism in Laojunshan of SE Yunnan, China: Geochemistry, geodynamic implication and related mineralization. Nanjing University, Jiangsu Sheng

Zeng ZG, Li CY, Liu YP, Tu GZ (1999) Geology and geochemistry of metamorphogenic skarn form Laojunshan metallogenic province. Acta Mineral Sin 19(1):48–55

Zhao B, Li TJ, Li ZP (1983) Experimental study of physico-chemical conditions of the formation of skarns. Geochimica 3:256–267

Zhao YM, Lin WW, Bi CS (1990) China skarn type deposit. Geology Publishing House, Beijing, pp 1–347

Zhou JP, Xu KQ, Hua RM, Zhao YY, Zhu JC (1998) Characteristics and genesis of exhalative sedimentary massive sulfides in southeastern Yunnan Province. Acta Mineral Sin 18(2):35–41

Zhou JX, Wang JS, Yang DZ, Liu JH (2013a) H–O–S–Cu–Pb isotopic constraints on the origin of the Nage Cu-Pb Deposit, Southeast Guizhou Province, SW China. Acta Geol Sin (Engl Ed) 87(5):1334–1343

Zhou JX, Huang ZL, Zhou MF, Li XB, Jin ZG (2013b) Constraints of C–O–S–Pb isotope compositions and Rb–Sr isotopic age on the origin of the Tianqiao carbonate-hosted Pb–Zn deposit, SW China. Ore Geol Rev 53(1):77–92

Zhou JX, Dou S, Huang ZL, Cui YL, Ye L, Li B, Gan T, Sun HR (2016) Origin of the luping Pb deposit in the beiya area, Yunnan Province, sw China: constraints from geology, isotope geochemistry and geochronology. Ore Geol Rev 72:179–190

Zijin Scheelite Industry Group Co., LTD (2014) Nanwenhe scheelite deposit resources reserve report in the Malipo, Yunnan